



Cite this: *RSC Adv.*, 2017, 7, 24856

Biocompatible and biodegradable solid polymer electrolytes for high voltage and high temperature lithium batteries

Yue Lin,^a Yun Cheng,^a Jie Li,^a Jan D. Miller,^b Jin Liu ^{*a} and Xuming Wang^{*b}

Solid polymer electrolytes (SPEs) have significant potential to improve the energy density of lithium batteries and exhibit good flexibility, electrochemical stability and increased safety. In this study, a biocompatible and biodegradable SPE is prepared by using the natural product, wheat flour. The SPE is found to have an ionic conductivity of $2.62 \times 10^{-5} \text{ S cm}^{-1}$ at 25 °C with a Li^+ ionic transference number of 0.51. FTIR and SEM are used to characterize the chemical and physical structures of the SPE. The results show that the enhanced ionic conductivity is mainly due to good compatibility of wheat flour with PEO and the decreased crystallinity of the electrolyte. Using the SPE, both NCM-811 and LiFePO_4 batteries can be used in the temperature range of 25–100 °C. The experimental results demonstrate the potential of nature-derived solid materials for high energy and high safety green energy storage systems.

Received 8th February 2017
 Accepted 29th April 2017

DOI: 10.1039/c7ra01601h

rsc.li/rsc-advances

1. Introduction

Modern applications of electrical systems require energy storage systems with high temperature, high energy, and high safety at the same time.^{1,2} However, most of the present batteries based on combustible organic solvents cannot simultaneously meet these requirements.³ This necessitates the discovery of solid electrolytes. Among advanced electrolytes, solid polymer electrolytes (SPEs) are fascinating due to their flexible properties, which enable the fabrication of batteries of various shapes.^{4–9} In this way, the overall battery packaging and cost can be reduced and the energy density enhanced.¹⁰ Besides, SPEs also make the use of high energy cathodes safer thanks to SPEs' high thermal and electrochemical stability. Thus, the energy density of SPE batteries can be increased.

SPE research began with polyethylene oxide (PEO) based electrolytes, which are also widely studied today.^{11–15} Various methods have been used to improve the ionic transport performance of these electrolytes including adding nanoparticles, crosslinking to make a new polymer host, and blending polymers.^{14–20} Recently, nanotube halloysite modified electrolytes were reported to achieve ionic conductivity of $1.11 \times 10^{-4} \text{ S cm}^{-1}$.¹⁷ By using the electrolyte, the all-solid-state lithium–sulfur battery obtained a capacity of 1350 mA h g^{-1} initially at 25 °C and 0.1C. Besides, micro size lithium ionic conductive ceramic $\text{Li}_{10}\text{GeP}_2\text{S}_{12}$ was used in a PEO electrolyte, which exhibited ionic conductivity of $1.18 \times 10^{-5} \text{ S cm}^{-1}$ and $1.21 \times 10^{-3} \text{ S cm}^{-1}$ at 25

and 80 °C, respectively.¹³ The $\text{LiFePO}_4/\text{Li}$ battery achieved capacities of 158, 148, 138 and 99 mA h g^{-1} at current rates of 0.1C, 0.2C, 0.5C and 1C at 60 °C, respectively. Our previous results show that a food grade starch hosted polymer electrolyte presents both high ionic conductivity of $3.39 \times 10^{-4} \text{ S cm}^{-1}$ and high lithium ion transference number of 0.80 at 25 °C.²¹ Finally, it was reported that a cellulose nonwoven membrane supported PEO:PCA:LiBOB SPE displayed ionic conductivity of $1.3 \times 10^{-5} \text{ S cm}^{-1}$ at 20 °C.²² These publications demonstrate the possibility of using natural materials for the design and fabrication of SPEs.

Natural materials are largely composed of carbon and oxygen, which are similar to $-\text{C}-\text{C}-\text{O}-$ units of PEO. Besides, PEO is biocompatible and hence has been widely used in pharmaceutical industries.²³ Therefore, it is expected that PEO will be compatible with natural materials.²⁴ The food grade natural materials for our daily life such as corn starch, wheat flour and protein powder are nano- to micro-sized powders with well controlled size. Thus, these products hold great potential as direct filler material in PEO based electrolytes.

Among these natural materials, wheat flour has been widely used to make dumplings because of its excellent filming properties.²⁵ In this study, food grade wheat flour was directly used to prepare a PEO electrolyte. The electrochemical and thermal properties of the solid polymer electrolyte were studied. The chemical and physical structures of the electrolyte were characterized to investigate the ionic transport. The wide temperature application potential of the biodegradable and biocompatible electrolyte was demonstrated by assembling the SPE into both high voltage $\text{Li}(\text{Ni}_{0.8}\text{Co}_{0.1}\text{Mn}_{0.1})\text{O}_2$ (NCM-811) and high safety LiFePO_4 batteries working in the temperature range of 25–100 °C.

^aSchool of Metallurgy and Environment, Central South University, Changsha, Hunan, 410083, China. E-mail: jinliu@csu.edu.cn

^bDepartment of Metallurgical Engineering, University of Utah, Salt Lake City, UT 84112, USA. E-mail: x.wang@utah.edu



2. Experimental

2.1 Materials

Polyethylene oxide (PEO, Mw = 4 000 000, 99.9%) and acetonitrile (CH₃CN, chromatographic grade) were obtained from Aladdin. Jinshahe brand wheat flour was bought from the supermarket. The wheat flour is mainly composed of wheat starch and protein. Lithium bis(trifluoro-methanesulfonyl) imide (LiTFSI, +99.5%) was purchased from Sigma-Aldrich and stored in a glove box before use.

2.2 Preparation of PEO + LiTFSI + wheat flour electrolyte

The preparation of the flexible SPE was carried out as follows. PEO and wheat flour were dried at 40 °C in vacuum for 24 h. The LiTFSI was used directly in an argon filled glove box. With all materials in the glove box, the PEO, wheat flour, LiTFSI and acetonitrile were stirred in a beaker until the mixture was uniform. Then the suspension was casted and dried to form a flexible PEO + LiTFSI + wheat flour electrolyte film at 80 °C in the glove box. The ratios of PEO, wheat flour and LiTFSI were adjusted to optimize the performance of the SPE.

2.3 Electrochemical properties of the SPE

Electrochemical impedance was used to measure the ionic conductivity of the SPE in the temperature range from 25 to 100 °C. The SPE films were sandwiched between two stainless steel (SS) disks and assembled into a CR2025 cell. The amplitude voltage was 10 mV and the frequency range was 100 kHz–1 Hz. The ionic conductivities were calculated as follows:

$$\sigma = \frac{l}{SR_b}$$

where l is the thickness of the SPE film, R_b is the resistance of the electrolyte, obtained from the intercept of the x -axis of the straight line, and S is the area of the blocking stainless steel electrodes.

Lithium ionic transference number was obtained by using the polarization method. The SPE was sandwiched between two lithium discs and assembled in a CR2025 cell. The cell was polarized with a voltage of 10 mV and the current changing with elapsed time was recorded. The impedances of the cell before and after polarization were measured.

Electrochemical stability of the SPE was tested by using stainless steel as the working electrode, and lithium as reference and counter electrodes. The cell consisting of the electrodes and SPE was sealed in CR2025 shells. Testing was conducted from open circuit voltage (OCV) to 6 V vs. Li/Li⁺ at a scan rate of 10 mV s⁻¹. Cyclic voltammetry of the Li/SPE/SS cell in the voltage route of OCV → -2 V → OCV at 25 °C and of OCV → -0.5 V → OCV at 100 °C at a scan rate of 10 mV s⁻¹ was used to investigate the plating/stripping performance of Li⁺/Li.

2.4 Thermal, physical and chemical structural characterization of the SPE

Morphologies of the wheat flour particles and solid polymer electrolyte were observed with a scanning electron microscopy

(SEM, JSM-6360LV) and the elemental distribution of the electrolyte sample was examined by energy dispersive spectrometer (EDS, EDX-GENESIS). The thermal behavior of the electrolyte was identified by thermogravimetric analysis (TGA, SDTQ600) under an Ar atmosphere at a heating rate of 10 °C min⁻¹ from room temperature to 800 °C. Additionally, combustion test was carried out to characterize the flame-retardant ability of the electrolyte. The SPE or Celgard separator used with liquid organic electrolyte was placed near to the flame and the results were recorded by camera. Attenuated total reflectance Fourier transform infrared spectroscopy (ATR-FTIR, Bruker Tensor II) was performed to analyze the chemical structure of the electrolyte film.

2.5 Battery performance

Batteries based on the SPE were assembled and sealed in CR2025 coin cells by contacting in sequence a NCM-811 or LiFePO₄ cathode ($d = 10$ mm), a layer of SPE, and a lithium metal anode disk ($d = 15.6$ mm, thickness = 0.3 mm). The electrode–electrolyte was housed and sealed in a CR2025 coin cell. The cathode was prepared by making NCM-811 or LiFePO₄, binder and carbon with weight ratio of 8 : 1 : 1 into NMP slurry. The slurry was coated on aluminum foil and heated at 100 °C to remove the solvent. The cathode was cut into discs. The batteries were assembled in the argon filled glove box. The cut-off voltage of the discharge and charge process for LiFePO₄ battery was respectively 2.0 and 4.2 V at 25 °C, 2.0 and 3.8 V at 100 °C. The cut-off voltage of the discharge and charge process of NCM-811 battery was respectively 2.5 and 4.2 V at both 25 and 100 °C. Rate performance of the batteries at 100 °C was conducted at 1, 3, 5, 10C and back to 5, 3, 1C. In each rate, the battery was cycled for 5 times. All the tests were performed in a LAND CT2001A battery test system.

3. Results and discussion

3.1 Lithium ionic conductivity, chemical structure and morphology of the wheat flour modified SPE

As a crucial parameter, the ionic conductivity of the PEO + LiTFSI + wheat flour SPE was optimized by adjusting the weight ratio of PEO, wheat flour and LiTFSI, and the results are shown in Fig. 1.

In Fig. 1a, the ionic conductivities of the SPEs at 25 °C with PEO : wheat flour weight ratio of 10 : 1, 9 : 1 and 4 : 1 and LiTFSI weight concentration of 20%, 30%, 40% and 50% are shown. Further increase in the weight of wheat flour leads to rupture of the film. So the PEO : wheat flour weight ratio was kept higher than 4 : 1. It is seen that at the LiTFSI concentrations of 30%, 40%, and 50%, the SPEs with PEO : wheat flour ratio of 9 : 1 exhibit highest ionic conductivities compared with those with PEO : wheat flour ratio of 10 : 1 and 4 : 1. At low LiTFSI concentration of 20%, the SPEs with all PEO : wheat flour ratios have almost the same ionic conductivity of about 2.12×10^{-6} S cm⁻¹.

The ionic conductivity increases with LiTFSI content for each PEO : wheat flour ratio at first. At 40%, the SPEs present



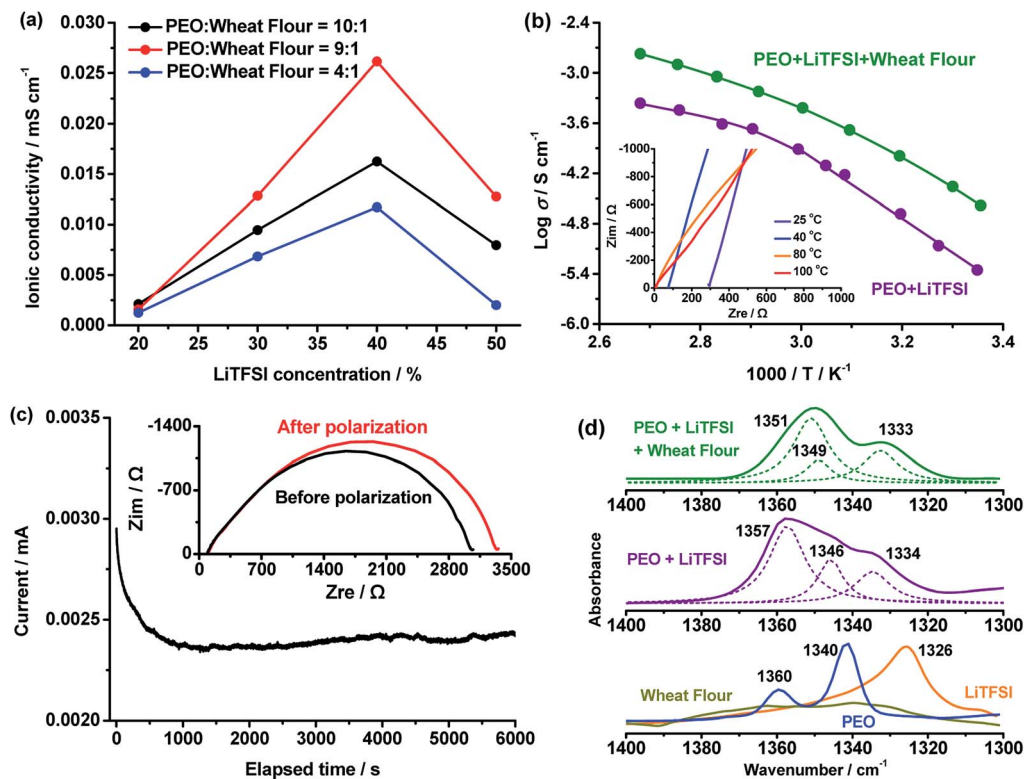


Fig. 1 (a) Ionic conductivity of the SPEs at 25 °C with PEO : wheat flour weight ratio of 10 : 1, 9 : 1 and 4 : 1 and LiTFSI weight concentration of 20%, 30%, 40% and 50%. (b) Ionic conductivity as a function of temperature of the SPE with PEO : wheat flour weight ratio of 9 : 1 and LiTFSI concentration of 40%. Inset is the EIS spectra at some selected temperatures for ionic conductivity calculation. The ionic conductivity of PEO + LiTFSI SPE with LiTFSI concentration of 40% is also shown as comparison. (c) Chronoamperometry of the Li/SPE/Li cell at a potential step of 10 mV. Inset: the AC impedance spectra of the same cell before polarization and after the steady-state current. (d) ATR-FTIR spectra of PEO, wheat flour, LiTFSI, PEO + LiTFSI and PEO + LiTFSI + wheat flour. The spectra of PEO + LiTFSI and PEO + LiTFSI + wheat flour were fitted with the same half-width of the peaks at 1360 cm⁻¹ and 1340 cm⁻¹ in PEO spectrum and 1326 cm⁻¹ in LiTFSI spectrum.

the highest value. When the content is raised to 50%, the ionic conductivities decline. The highest ionic conductivity of the SPEs is $2.62 \times 10^{-5} \text{ S cm}^{-1}$ and is obtained at PEO : wheat flour ratio of 9 : 1 and LiTFSI concentration of 40%. The optimal conditions were maintained in the following measurements.

Previous research on PEO based electrolyte shows that the ionic conductivity was higher in the amorphous state than in the crystalline state because of a better segment motion leading to quicker carriers' movement.^{26,27} In the crystalline state, the logarithm ionic conductivity shows a linear relation with $1000/T$, which obeys the Arrhenius equation ($\sigma = A \exp \frac{E_a}{RT}$).²⁸ In amorphous state, the Vogel–Tamman–Fulcher equation (VTF, $\sigma = AT^{-0.5} \exp \left[-\frac{B}{\kappa(T - T_0)} \right]$) can describe the ionic conductivity behavior.²⁸ So, the ionic conductivities of the PEO + LiTFSI + wheat flour with highest room temperature ionic conductivity were measured at different temperatures to investigate the physical state of the SPE and the results are shown in Fig. 1b. The EIS spectra for calculation at some selected temperatures are present in the inset of Fig. 1b. The ionic conductivity of PEO + LiTFSI without wheat flour is also shown in Fig. 1b as comparison. At 25 °C, the ionic conductivity of PEO + LiTFSI + wheat flour electrolyte is $2.62 \times 10^{-5} \text{ S cm}^{-1}$, which is

6 times of that of PEO + LiTFSI electrolyte ($4.47 \times 10^{-6} \text{ S cm}^{-1}$). Besides, it is found that for PEO + LiTFSI electrolyte, the logarithm ionic conductivity shows a linear relation with $1000/T$ at low temperature, while a curve relation at high temperature. After fitted the data with the Arrhenius equation at low temperature and the VTF equation at high temperature, there is an inflection point at 60 °C corresponding to phase transition (crystalline to amorphous) of PEO. As a comparison, the ionic conductivity of PEO + LiTFSI + wheat flour changes smoothly with temperature. These results mean that the crystalline state almost disappears in the wheat flour modified SPE, which benefit for ionic transportation.

Lithium ionic transference number was measured by polarization and AC impedance to evaluate the Li⁺ ion contribution for the total ionic conductivity²⁹ and the results are presented in Fig. 1c. The value was calculated by the following expression:³⁰

$$t^+ = \frac{I_s(V - I_0 R_0)}{I_0(V - I_s R_s)}$$

where V is the DC voltage applied to the cell, 10 mV in this test; R_0 and R_s are the initial and steady-state interfacial resistances, 2946.6 and 3230.6 Ω respectively herein; and I_0 and I_s are the initial and steady-state current, 0.00296 and 0.00246 mA respectively. So, the lithium ionic transference number



calculated is 0.51. Compared to the pure PEO + LiTFSI system, the value is greatly enhanced.^{31,32} This value is also higher than 0.2–0.4 of commercial liquid electrolytes.^{33,34}

It is generally accepted that the ionic conductivity of SPEs is decided by the number of charge carriers and the carrier mobility.²⁸ The addition of wheat flour decreases the crystallinity of the electrolyte. So, at low flour concentration, the ionic conductivity increases with flour, while further increases in flour concentration leads to the decline of PEO segment motion and ionic conductivity decreases. Besides, the ionic conductivity is also affected by LiTFSI concentration, which influences the number of Li⁺ ions. At low LiTFSI concentration, the ionic conductivity is simply improved by increasing the number of carriers. When the concentration of lithium salt is high, the ion pairs begin to form and the ionic conductivity is declined. In addition, from the Li⁺ ionic transference number result, it is suspected that the wheat flour also contributes to the dissociation of the LiTFSI salt and improves the pure lithium ionic conductivity.

Chemical structure and morphology of the PEO + LiTFSI + wheat flour SPE was investigated to further understand the ionic conductivity improvement in the SPE. The chemical structure of the wheat flour modified SPE was investigated by ATR-FTIR. Fig. 1d shows the FTIR spectra at 1400–1300 cm⁻¹ of pure PEO, pure LiTFSI, wheat flour, PEO + LiTFSI and PEO + LiTFSI + wheat flour SPE. For pure PEO, there are two peaks at 1360 and 1340 cm⁻¹, which are from wagging absorptions of –CH₂– in the helical structure and the trans planar structure, respectively.³⁵ The appearance of these two –CH₂– vibrations in PEO illustrates that crystalline structures are present.^{36,37} For wheat flour there are also absorptions in 1360 and 1340 cm⁻¹. The peak at 1326 cm⁻¹ in LiTFSI spectrum is from asymmetric –SO₂– stretching.³⁸ After mixing PEO with LiTFSI, the peak shift of PEO at 1360 cm⁻¹ to 1357 cm⁻¹, 1340 cm⁻¹ to 1346 cm⁻¹ and the peak shift of –SO₂– at 1326 cm⁻¹ in LiTFSI to 1334 cm⁻¹ prove that dissociation of LiTFSI by PEO occurs. After addition of wheat flour to PEO + LiTFSI, the two peaks of –CH₂– in PEO further shift to 1351 cm⁻¹ and 1349 cm⁻¹. The peak of –SO₂– remains almost the same. These results demonstrate that the wheat flour particles interact with PEO and change the crystalline structure. Thus, the ionic conductivity is enhanced by reducing the crystallinity.

The morphology and elemental distribution of the wheat flour modified SPE were studied respectively by SEM and EDS, and the results are seen in Fig. 2. The wheat flour particles present diameters of 1–10 μm in Fig. 2a. After mixing PEO, LiTFSI and wheat flour in acetonitrile and cast in argon filled glove box, a film with quite a smooth surface (see Fig. 2b) was formed. Only some small particles with diameter of about 1 μm are found on the surface. Fig. 2a and b were obtained at the same magnification. Therefore, the wheat flour particles can be well dispersed in the SPE film.

From the EDS results, the elements of O and S (Fig. 2c and d respectively) are uniformly distributed in the PEO + LiTFSI + wheat flour SPE. These results demonstrate that the three components of PEO, wheat flour and LiTFSI are compatible and well dispersed in the SPE. Wheat starch and protein are two

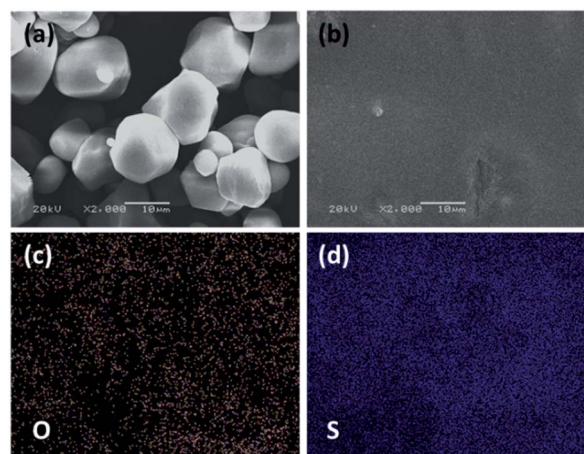


Fig. 2 Morphology and elemental distribution in wheat flour modified SPE. (a) SEM image of wheat flour particles, (b) SEM image of PEO + LiTFSI + wheat flour SPE, (c) O and (d) S elemental distribution in the SPE.

main compositions in wheat flour.³⁹ In previous reports, it is found that SiO₂, Al₂O₃, MOF and halloysite fillers can reduce PEO crystallinity, and Li⁺ ion channel is formed by the interaction of PEO, fillers and lithium salt.^{16,17,31,32} There are plenty of –C–O–, –N– and –C=O functional groups in wheat flour, which can coordinate with Li⁺ ions like –C–O–C– in PEO. Thus, special Li⁺ ion channels on the surface of wheat flour particles are formed. In addition, the interactions reduce the crystallinity of PEO. Therefore, the Li⁺ ionic conductivity is enhanced.

3.2 Thermal and electrochemical stability of the SPE

Thermal and electrochemical stability of the SPE were tested to decide the application temperature and voltage range of the SPE. Thermal stability was characterized by thermal analysis and combustion test, and the results are presented in Fig. 3.

Thermal degradation of the SPE is seen in Fig. 3a. Below 270 °C, the electrolyte has a weight loss of about 2.0%. This may be due to the water absorbed during sample transfer. The first degradation from 270 to 362 °C with a weight loss of 5.0% comes from the decomposition of wheat flour. The main weight

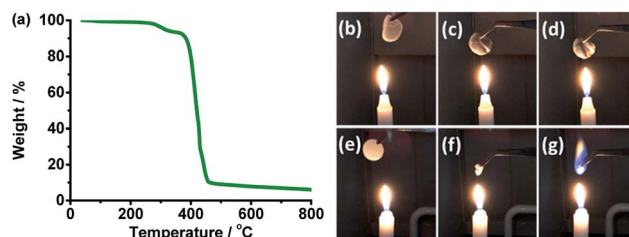


Fig. 3 Thermal stability characterization of the wheat flour modified SPE. (a) Thermal analysis of the SPE. The SPE (b) was placed close to the flame, the electrolyte at (c) and (d) were still self-standing after 10 seconds. As a comparison, the Celgard separator with liquid organic electrolyte (e) was also placed close to the flame and stopped at almost the same position with SPE, (f) the separator shrunk in less than 1 second and (g) the electrolyte burned.



loss of about 83% from 362 to 460 °C corresponds to the decomposition of PEO and LiTFSI.^{40,41} The residual of 10% may be carbon materials.

Combustion test shows a flame retardant ability of the wheat flour modified SPE. When the SPE (Fig. 3b) was placed close to

the flame, the electrolyte was still in a self-standing film state and did not burn (Fig. 3c and d). As a comparison, when the Celgard separator with liquid organic electrolyte (Fig. 3e) was also placed near the flame and at almost the same position above the flame with SPE in Fig. 3c, the separator shrunk quickly (Fig. 3f) and the electrolyte burned (Fig. 3g).

Fig. 4a and b shows linear sweep and cyclic voltammetry results at 25 and 100 °C to evaluate the electrochemical stability of the wheat flour modified SPE. The electrolyte began experiencing decomposition from 5.5 and 5.1 V at 25 and 100 °C respectively in the positive scan. Both of these values are higher than the decomposition voltage of commercial liquid organic electrolytes (~4.2 V). The value at 100 °C is also higher than that of PEO + LiTFSI,¹⁷ showing that the electrochemical stability was enhanced by wheat flour. Besides, the plating/stripping of Li⁺/Li at near 0 V was investigated by cycling the SPE in the voltage route of OCV → -2 V → OCV at 25 °C and OCV → -0.5 V → OCV at 100 °C. This once again validates the lithium ionic transfer ability in the wheat flour modified SPE in the temperature range of 25 to 100 °C.

These results indicate good thermal and electrochemical stability of the wheat flour modified electrolyte. The SPE is able to be applied in the battery with high voltage and high temperature.

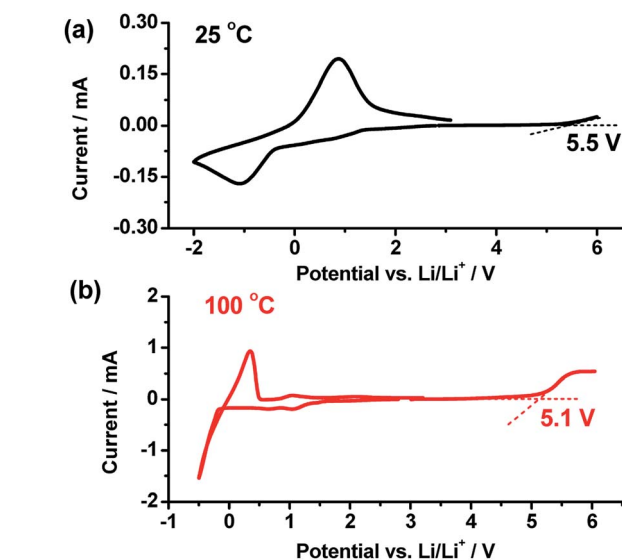


Fig. 4 Linear sweep and cyclic voltammetry results at (a) 25 °C and (b) 100 °C. The negative scan OCV → -2 V → OCV and OCV → -0.5 V → OCV at respectively 25 °C and 100 °C, and the positive scan OCV → 6 V at a rate of 10 mV s⁻¹ were conducted.

3.3 LiFePO₄ battery performance at 25 and 100 °C

The optimal SPE films with PEO : wheat flour ratio of 9 : 1 and LiTFSI concentration of 40% were used to fabricate all-solid-

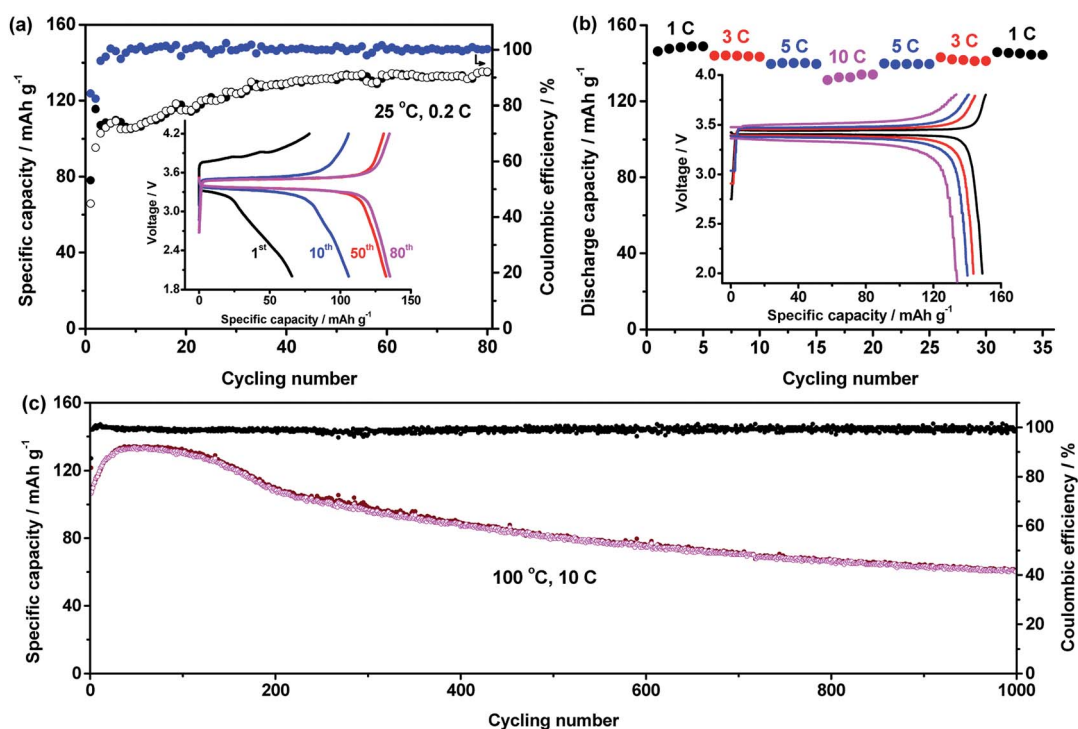


Fig. 5 Cycling performance of LiFePO₄/SPE/Li battery at (a) 25 °C and 0.2C, inset is the charge/discharge curve at 1st, 10th, 50th, and 80th cycle, (b) different rates of 1C (black), 3C (red), 5C (blue), and 10C (pink) at 100 °C, inset presents the charge/discharge curves at different rates and (c) 100 °C and 10C.



state $\text{LiFePO}_4/\text{Li}$ batteries, the performance of which is shown in Fig. 5. At 25 °C and 0.2C, the capacity of the battery increases with cycling number in Fig. 5a. After 50 cycles, a stable value of about 130 mA h g^{-1} was obtained. After 80 cycles, the capacity still retained 135.2 mA h g^{-1} . At stable cycling state, the battery presents a discharge plateau at 3.37 V.

High temperature performance of the battery was also tested. In Fig. 5b, a battery was cycled at various C-rates of 1C, 3C, 5C, 10C and back to 5C, 3C and 1C to investigate the rate performance of the battery at 100 °C. The average capacities at these rates are respectively 148.0 ± 1.1 , 144.8 ± 0.3 , 139.9 ± 0.3 , 132.3 ± 1.2 , 139.6 ± 0.2 , 141.8 ± 0.8 , and 145.0 ± 0.6 mA h g^{-1} . The charge/discharge curves of the battery at different rates are seen in the inset of Fig. 5b. The discharge voltage at 1C, 3C, 5C and 10C are respectively 3.42, 3.39, 3.37 and 3.34 V. The recovery of the capacity and high discharge voltage even at high rate of 10C reveal excellent rate performance of the battery.

The cycling performance of the battery at high temperature of 100 °C and high rate of 10C are shown in Fig. 5c. The battery had an initial discharge capacity of 109.8 mA h g^{-1} . After about 40 cycles, highest capacity of 133.7 mA h g^{-1} was obtained. After 1000 cycles, the capacity of 60.2 mA h g^{-1} was retained.

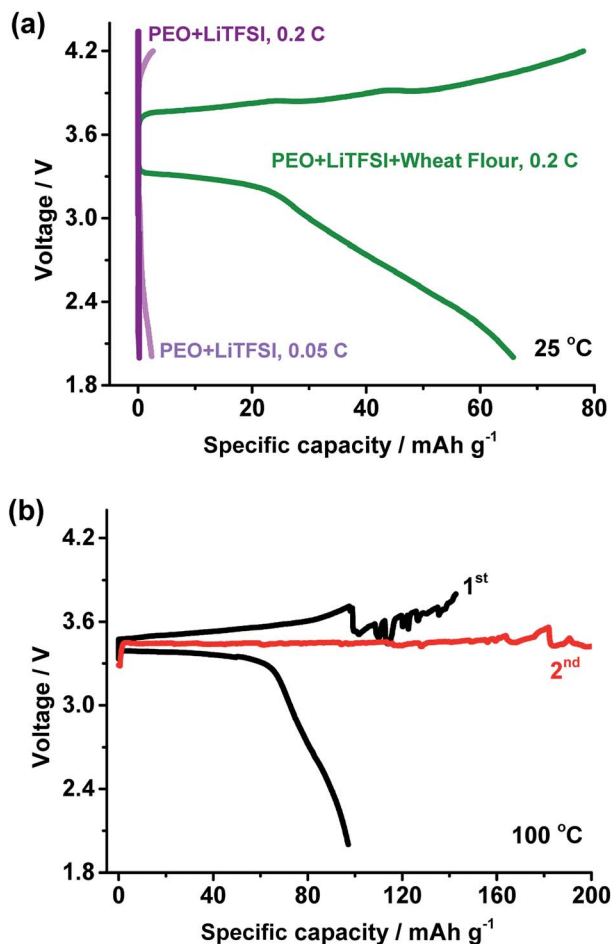


Fig. 6 (a) Charge/discharge curves of PEO + LiTFSI and PEO + LiTFSI + wheat flour based LiFePO_4 battery at 25 °C and (b) charge/discharge curves of PEO + LiTFSI based LiFePO_4 battery at 100 °C and 1C.

The performance of $\text{LiFePO}_4/\text{Li}$ battery with unmodified PEO + LiTFSI SPE was tested at 25 °C and 100 °C. In Fig. 6a at 25 °C and 0.2C, the battery cannot be charged. When the current rate changed to 0.05C, the battery can be charged. But the capacity of about 2.3 mA h g^{-1} is much lower than that of the PEO + LiTFSI + wheat flour based battery. This may be caused by the poor ionic conductivity of the PEO + LiTFSI electrolyte at room temperature.

In addition, two PEO + LiTFSI based batteries were cycled at 100 °C and 1C. The voltage of one battery quickly dropped to almost 0 V. The cycling performance of another battery is presented in Fig. 6b. The battery had a charge and discharge capacity of 142.7 mA h g^{-1} and 97.2 mA h g^{-1} in the 1st cycle with an efficiency of only 68.1%. The battery cannot be full charged in the second cycle. It is suggested that short circuit or micro short circuit happened in the battery at 100 °C. The poor mechanical stability of PEO + LiTFSI may be the reason for the short circuit. These results reveal wide temperature and high rate ability of PEO + LiTFSI + wheat flour SPE based battery.

3.4 NMC-811 battery performance at 25 and 100 °C

The wheat flour SPE was also used to match NMC-811 cathode to make a high voltage all-solid-state lithium battery. The performances at both 25 and 100 °C were investigated. The highest discharge capacity of the battery at 25 °C and 0.1C (Fig. 7a) was 133 mA h g^{-1} . After 60 cycles, the capacity of 62.9 mA h g^{-1} was retained. EIS was used to investigate the capacity decay of this battery and the spectra are shown in the inset of Fig. 6a. The bulk resistances of the battery before cycling, after 1st cycle, after 4th cycle and after 60 cycles were respectively 626, 474, 525 and 149 Ω . The interfacial resistances were respectively 2053, 1079, 1245 and 2555 Ω . The decrease in both bulk and interfacial resistances after the 1st cycle may be the reason for increasing capacity at the initial cycles. However, the interfacial resistance increased with further cycling, which may be the reason for the subsequent decrease in capacity.

Rate performance of the NCM-811 battery at 100 °C was carried out, which can be seen in Fig. 7b. The capacities at 1C, 3C, 5C, 10C, 5C, 3C and 1C were respectively 145.74 ± 10.0 , 80.2 ± 8.6 , 38.5 ± 3.85 , 9.6 ± 0.5 , 24.1 ± 2.6 , 34.5 ± 2.6 and 67.5 ± 3.8 mA h g^{-1} . Additionally, the charge/discharge curves at different rates can be seen in the inset of Fig. 7b. Quick increase in charge voltage and decrease in discharge voltage by increasing rate present. This rate performance is not as good as that of the LiFePO_4 battery.

It is suspected that the capacity decay of NCM-811 battery may be caused by the instability of the NCM-811 cathode and the compatibility (electrochemical, chemical and physical stability) at the NMC-811/SPE interface. Because both the LiFePO_4 and NCM-811 batteries were cycled inside the decomposition voltage range of the SPE, the SPE did not decompose. Improvement on the stability of NCM-811 cathode and the NCM/SPE interface is necessary to improve the battery performance.



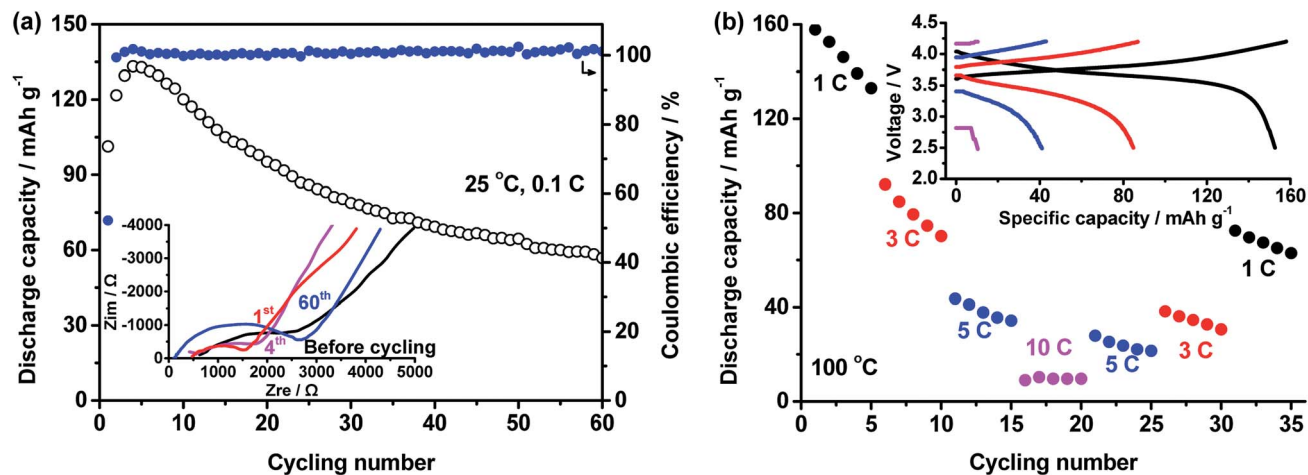


Fig. 7 (a) Cycling performance of the NCM-811/SPE/Li battery at 25 °C and 0.1C. Inset shows the EIS spectra of the battery before cycling, after 1st cycle and after 60 cycles. (b) Rate performance of the NCM-811/SPE/Li battery at 100 °C. Inset presents the charge/discharge curves at different rates.

4. Conclusions

In this work, natural product wheat flour was directly used to prepare SPEs. Due to the interaction of the flour with PEO and LiTFSI, the crystallinity of the SPE is reduced. Thus, the lithium ionic conductivity is greatly increased. With the low cost electrolyte, the all-solid-state NCM-811 and LiFePO₄ batteries can work from 25 to 100 °C. Especially, the LiFePO₄ battery is able to obtain capacity of 132.3 mA h g⁻¹ at high rate of 10C and a good cycling performance. The results with the wheat flour demonstrate an efficient way to apply biocompatible SPEs with various cathodes and realize a wide temperature range application at low cost as well as micro-scale batteries for devices in organisms at high safety.

Acknowledgements

We acknowledge support from the National Natural Science Foundation of China (No. 51274239), Chinese Academy of Engineering (2016-XY-18) and the Fundamental Research Funds from the Central Universities for Central South University (No. 2015zsts036).

References

- 1 E. C. Evarts, *Nature*, 2015, **526**, S93–S95.
- 2 X. R. Lin, M. Salari, L. M. R. Arava, P. M. Ajayan and M. W. Grinstaff, *Chem. Soc. Rev.*, 2016, **45**, 5848–5887.
- 3 P. Hu, J. Chai, Y. Duan, Z. Liu, G. Cui and L. Chen, *J. Mater. Chem. A*, 2016, **4**, 10070–10083.
- 4 Y. Liu, S. Gorgutsa, C. Santato and M. Skorobogatiy, *J. Electrochem. Soc.*, 2012, **159**, A349–A356.
- 5 R. J. Chen, W. J. Qu, X. Guo, L. Li and F. Wu, *Mater. Horiz.*, 2016, **3**, 487–516.
- 6 W. He, Z. Cui, X. Liu, Y. Cui, J. Chai, X. Zhou, Z. Liu and G. Cui, *Electrochim. Acta*, 2017, **225**, 151–159.
- 7 J. Zhang, C. Ma, J. Liu, L. Chen, A. Pan and W. Wei, *J. Membr. Sci.*, 2016, **509**, 138–148.
- 8 Y. Zhang, W. Cai, R. Rohan, M. Pan, Y. Liu, X. Liu, C. Li, Y. Sun and H. Cheng, *J. Power Sources*, 2016, **306**, 152–161.
- 9 W. Liu, N. Liu, J. Sun, P.-C. Hsu, Y. Li, H.-W. Lee and Y. Cui, *Nano Lett.*, 2015, **15**, 2740–2745.
- 10 L. Porcarelli, C. Gerbaldi, F. Bella and J. R. Nair, *Sci. Rep.*, 2016, **6**, 19892.
- 11 D. E. Fenton, J. M. Parker and P. V. Wright, *Polymer*, 1973, **14**, 589.
- 12 B. Chen, Q. Xu, Z. Huang, Y. Zhao, S. Chen and X. Xu, *J. Power Sources*, 2016, **331**, 322–331.
- 13 Y. Zhao, C. Wu, G. Peng, X. Chen, X. Yao, Y. Bai, F. Wu, S. Chen and X. Xu, *J. Power Sources*, 2016, **301**, 47–53.
- 14 D. Lin, W. Liu, Y. Liu, H. R. Lee, P.-C. Hsu, K. Liu and Y. Cui, *Nano Lett.*, 2016, **16**, 459–465.
- 15 Y. Zhang, J. Lai, Y. Gong, Y. Hu, J. Liu, C. Sun and Z. L. Wang, *ACS Appl. Mater. Interfaces*, 2016, **8**, 34309–34316.
- 16 F. Croce, G. B. Appetecchi, L. Persi and B. Scrosati, *Nature*, 1998, **394**, 456–458.
- 17 Y. Lin, X. Wang, J. Liu and J. D. Miller, *Nano Energy*, 2017, **31**, 478–485.
- 18 D. Luo, Y. Li, W. Li and M. Yang, *J. Appl. Polym. Sci.*, 2008, **108**, 2095–2100.
- 19 H. Ben youcef, O. Garcia-Calvo, N. Lago, S. Devaraj and M. Armand, *Electrochim. Acta*, 2016, **220**, 587–594.
- 20 X.-X. Zeng, Y.-X. Yin, N.-W. Li, W.-C. Du, Y.-G. Guo and L.-J. Wan, *J. Am. Chem. Soc.*, 2016, **138**, 15825–15828.
- 21 Y. Lin, J. Li, K. Liu, Y. Liu, J. Liu and X. Wang, *Green Chem.*, 2016, **18**, 3796–3803.
- 22 J. Zhang, L. Yue, P. Hu, Z. Liu, B. Qin, B. Zhang, Q. Wang, G. Ding, C. Zhang, X. Zhou, J. Yao, G. Cui and L. Chen, *Sci. Rep.*, 2014, **4**, 6272.
- 23 L. L. Ma, L. Deng and J. M. Chen, *Drug Dev. Ind. Pharm.*, 2014, **40**, 845–851.
- 24 F. Yu, K. Prashantha, J. Soulestin, M.-F. Lacrampe and P. Krawczak, *Carbohydr. Polym.*, 2013, **91**, 253–261.



- 25 X. Li, Y. Lv, Y. Chen and J. Chen, *Int. J. Food Prop.*, 2016, **19**, 1566–1582.
- 26 B. Kumar, S. J. Rodrigues and S. Koka, *Electrochim. Acta*, 2002, **47**, 4125–4131.
- 27 W. A. Henderson and S. Passerini, *Electrochem. Commun.*, 2003, **5**, 575–578.
- 28 M. A. Ratner, P. Johansson and D. F. Shriver, *MRS Bull.*, 2000, **25**, 31–37.
- 29 F. B. Dias, L. Plomp and J. B. J. Veldhuis, *J. Power Sources*, 2000, **88**, 169–191.
- 30 J. Evans, C. A. Vincent and P. G. Bruce, *Polymer*, 1987, **28**, 2324–2328.
- 31 C. Capiglia, P. Mustarelli, E. Quartarone, C. Tomasi and A. Magistris, *Solid State Ionics*, 1999, **118**, 73–79.
- 32 K. Zhu, Y. Liu and J. Liu, *RSC Adv.*, 2014, **4**, 42278–42284.
- 33 D. Zhou, Y.-B. He, R. Liu, M. Liu, H. Du, B. Li, Q. Cai, Q.-H. Yang and F. Kang, *Adv. Energy Mater.*, 2015, **5**, 201500353.
- 34 S. Zugmann, M. Fleischmann, M. Amereller, R. M. Gschwind, H. D. Wiemhöfer and H. J. Gores, *Electrochim. Acta*, 2011, **56**, 3926–3933.
- 35 S. Yang, Z. Liu, Y. Liu and Y. Jiao, *J. Mater. Sci.*, 2015, **50**, 1544–1552.
- 36 I. Pucić and T. Jurkin, *Radiat. Phys. Chem.*, 2012, **81**, 1426–1429.
- 37 X. Li and S. L. Hsu, *J. Polym. Sci., Polym. Phys. Ed.*, 1984, **22**, 1331–1342.
- 38 L. J. Hardwick, J. A. Saint, I. T. Lucas, M. M. Doeff and R. Kostecki, *J. Electrochem. Soc.*, 2009, **156**, A120–A127.
- 39 C. M. Rosell, R. Altamirano-Fortoul, C. Don and A. Dubat, *Cereal Chem.*, 2012, **90**, 89–100.
- 40 R. R. Madathilal and S. L. Wunder, *Thermochim. Acta*, 2011, **523**, 182–186.
- 41 Z. Lu, L. Yang and Y. Guo, *J. Power Sources*, 2006, **156**, 555–559.

